Observational Study

Medicine

OPEN

Identification of pyroptosis-related gene signature for predicting prognosis of patients with pancreatic cancer using bioinformatics

Zhongbo Xu, MS[a], Wenyan Yu, MD[b], Lin Li, MD[a], Guojuan Wang, MD[c,*]

Abstract

Pancreatic cancer, a common digestive system malignancy, is dubbed the "king of cancers". The role of pyrophosis-related genes (PRGs) in pancreatic cancer prognosis is yet unknown. In pancreatic cancer and normal tissue, we discovered 9 PRGs that are expressed differently in pancreatic cancer and healthy tissue. Based on the differential expression of PRGs, 2 clusters of pancreatic cancer cases could be identified. The 2 groups had significant disparities in total survival time. The prognostic model of a 5-PRGs signature was created using least absolute shrinkage and selection operator (LASSO) method. The median risk score was used to split pancreatic cancer patients in The Cancer Genome Atlas (TCGA) cohort into 2 groups: low risk and high risk. Patients classified as low-risk had significantly higher survival rates than those classified as high-risk ($P < .01$). The same results were obtained by validating them against the Gene Expression Omnibus database ($P = .030$). Cox regression statistical analysis showed that risk score was an independent predictor of overall survival in pancreatic cancer patients. Functional enrichment analysis revealed that apoptosis, cell proliferation, and cell cycle-related biological processes and signaling pathways were enriched. Additionally, the immunological status of the high-risk group worsened. In conclusion, a novel pyroptosis-related gene signature can be used to predict pancreatic cancer patient prognosis.

Abbreviations: DEGs = extracted differentially expressed genes, GEO = Gene Expression Omnibus, LASSO = least absolute shrinkage and selection operator, OS = overall survival, PC = pancreatic cancer, PCA = principal component analysis, PRGs = pyroptosis-related genes, ROC = receiver operating characteristic, TCGA = The Cancer Genome Atlas, t-SNE = t-distributed stochastic neighbor embedding.

Keywords: gene signature, overall survival, pancreatic cancer, prognosis, pyroptosis

1. Introduction

Pancreatic cancer (PC) is a highly severe and malignant tumor of the digestive system with an inferior prognosis, and its morbidity and mortality have risen considerably in recent years.[1] According to data released by the American Cancer Society in 2019, PC-related mortality is the fourth highest among all malignancies.[2] Moreover, in recent years, lifestyle changes in developing countries, such as increased smoking rates, increased intake of high-calorie foods, and lack of physical activity, have led to a gradual increase in PC mortality.[3] Due to the insidious onset of PC, the initial stage often lacks specific clinical symptoms and indicators, and the high malignancy progresses rapidly. Thus, most patients are in advanced stages when they are admitted to the hospital. Complete tumor resection remains the most important treatment for PC, but only 15% to 20% of patients are able to undergo immediate surgery at initial diagnosis.[4] Even after tumor resection, the long-term survival of patients remains limited, and surgical resection plus adjuvant chemotherapy is currently the main treatment option.[5] Given the limits of current PC therapy, innovative targeted treatments and credible novel prognostic models are urgently needed to help patients live longer.

Pyroptosis is a relatively recent kind of cell death that is characterized by the creation of intracellular holes mediated by gasdermin family proteins, which cause cell swelling and rupture, the release of inflammatory mediators such as interleukin (IL)-1β, IL-18, and high mobility group box protein 1, and inflammatory responses.[6] It is now clear that gasdermin family proteins are the sole executors of cell pyroptosis, and activation of their N-terminal structural domain is sufficient to induce cell membrane pore formation and lead to the onset of pyroptosis.[7,8] The characteristic changes in the nucleus after the onset of pyroptosis are similar to those of apoptosis, such as nuclear crinkling

The National Natural Science Foundation of China (82160925) and Natural Science Foundation of Jiangxi,China(20202BAB216040, 20202BAB206069) sponsored this researchThe National Natural Science Foundation of China (82160925) and the Jiangxi Province Natural Science Foundation (20202BAB216040, 20202BAB206069) sponsored this research.

The authors have no conflicts of interest to disclose.

The datasets generated during and/or analyzed during the current study are publicly available.

[a] Emergency Department, Affiliated Hospital of Jiangxi University of Chinese Medicine, Nanchang, Jiangxi, China, [b] The Research Center for Differentiation and Development of Basic Theories of Chinese Medicine, Jiangxi University of Chinese Medicine, Nanchang, Jiangxi, China, [c] Department of Oncology, Affiliated Hospital of Jiangxi University of Chinese Medicine, Nanchang, Jiangxi, China.

**Correspondence: Guojuan Wang, Department of Oncology, Affiliated Hospital of Jiangxi University of Chinese Medicine, No.445, Bayi Avenue, Nanchang 330006, Jiangxi, China (e-mail: guojuan.wang@jxutcm.edu.cn).*

How to cite this article: Xu Z, Yu W, Li L, Wang G. Identification of pyroptosis-related gene signature for predicting prognosis of patients with pancreatic cancer using bioinformatics. Medicine 2022;101:41(e31043).

Received: 5 May 2022 / Received in final form: 2 September 2022 / Accepted: 7 September 2022

http://dx.doi.org/10.1097/MD.0000000000031043

and chromatin deoxyribo nucleic acid breakage and degradation.[9] When pyroptosis occurs, numerous pores appear in the cell membrane, causing permeable cell swelling, and the swollen cells eventually disintegrate, releasing a large amount of cellular inflammatory contents and rapidly stimulating the inflammatory response of the organism. Initially believed to be a critical mechanism in the anti-infection response, a rising amount of research has demonstrated that it is critical in the formation of malignancies.[10,11] Gasdermin D (GSDMD), a key protein involved in pyroptosis, may inhibit proliferation of gastric cancer cells by inhibiting the extracellular signal-regulated kinase, signal transducer and activator of transcription 3, and phosphatidylinositol 3-kinase (PI3K) pathways, and consequently the CyclinA2/cyclin-dependent kinase 2 complex, leading to cell cycle S/G_2 phase arrest.[12] Moreover, it has been found that malignant tumor cells stimulated by apoptosis-inducing chemotherapeutic drugs can inhibit tumor growth by activating the apoptosis regulator-BAX/caspase-3/Gasdermin-E signaling pathway to shift the cells from performing apoptosis to pyroptosis.[13]

With the continuous research, it is found that pyroptosis plays an important role in both the development of tumors. Pyroptosis on tumorigenesis as well as treatment is a hot topic of research in recent years. However, the prognostic value of pyroptosis-related genes (PRGs) in pancreatic cancer has not been elucidated. Therefore, we evaluated the expression of PRGs in normal and pancreatic cancer organs using bioinformatics tools to investigate their prognostic significance and the relationship between pyrogenesis and tumor immune status.

2. Materials and Methods

Because the data used in this study were collected from a public database, no ethical approval or patient permission was necessary.

2.1. Acquiring and preparing data

The Cancer Genome Atlas (TCGA) (https://portal.gdc.cancer.gov/repository) database was used to retrieve RNA-sequence data for 182 samples and their associated clinical characteristics. Perl software was used to organize the downloaded transcriptome data and extract relevant clinical data. We got the external validation cohort's RNA-sequence data and survival information from the Gene Expression Omnibus (GEO) (https://www.ncbi.nlm.nih.gov/geo/) database. The transcriptomic data of the GSE57495 database deposited by Chen et al[14] included tissue samples from 63 patients with PC. The data analysis was standardized using the R 4.04 software package "limma".[15]

2.2. Identification of PRGs

Through a literature review,[16–20] we extracted 52 PRGs. TCGA PC genes were intersected with the genes to obtain PC-associated PRGs using R software. Differential expression analysis of these PRGs was performed according to the splitting criteria: $P < .05$ and |log FC| >1. These PRGs were visualized on heat maps drawn using R. The PRGs were entered into the STRING database[21] to develop a protein–protein interaction (PPI) network.

2.3. Analysis of consensus clustering

We conducted a consensus clustering study on PRGs using the R 4.04 software package "ConsensusClusterPlus".[22] The K-means algorithm was used in conjunction with the Spearman distance to produce clustering. The maximum number of clusters was set at nine. To explore the differences and stability among the different clusters, we performed survival analysis and differential analysis of clinical features in the clusters. The results are presented using a heat map and Kaplan–Meier (KM) curves.

2.4. Screening for prognostic-related PRGs

PRGs and TCGA survival data (survival time and survival status) were merged using the R software "limma" package. The connection between each PRGs and the TCGA cohort's survival status was determined using Cox regression analysis. Values with $P < .05$ were considered to be associated with prognosis, and a hazard ratio (HR) > 1 represented a negative association between the gene expression and prognosis, while HR < 1 represented the opposite.

2.5. Developing and validating prognostic model

TCGA data were used as the training group to construct the prognostic model, and the GEO data were used as the test group to verify the accuracy of the model. On the basis of these predictive PRGs, we performed the least absolute shrinkage and selection operator (LASSO)-Cox regression analysis (R package "GLMNET")[23] to identify the candidate genes and build a prognostic model, which was based on these genes. To calculate the risk score, apply the formula below:

$$\text{Risk Score} = \sum_{i}^{5} Xi \times Yi$$ (X: Coefficient values, Y: gene expression values).

According to the risk score, TCGA and GEO patients were categorized into low-risk and high-risk subgroups, and the overall survival (OS) times of the two subgroups were compared using KM analysis. For predicting the prognostic model's precision, principal component analysis (PCA), t-distributed stochastic neighbor embedding (t-SNE), and time receiver operating characteristic analysis (ROC) were used in conjunction with the "survival", "survminer", "tsne", and "time ROC" R packages in the R 4.04 software. Finally, we utilized Cox regression analyses, both univariate and multivariate, to evaluate if the risk score could be employed as an independent prognostic factor.

2.6. Functional enrichment analysis

The extracted differentially expressed genes (DEGs) in high- and low-risk categories of the TCGA and GEO cohorts were screened using the R program "limma". The "clusterProfiler" program in R software was used to conduct Gene Ontology (GO) and Kyoto Encyclopedia of Genes and Genomes (KEGG) analysis on these DEGs.[24] The single-sample gene set enrichment analysis (ssGSEA) was utilized to generate the scores of immunological cells and functions to assess immunological disparities across risk groups.

3. Results

3.1. Identification of PRGs

The levels of expression of 52 PRGs were compared in the TCGA cohort (4 normal samples and 178 tumor samples). Among them, we identified nine differentially expressed PRGs of which seven (*NLRC4*, *NLRP3*, *NOD2*, *PLCG1*, *PRKACA*, *TNF*, and *GZMA*) were downregulated, while 2 (*CHMP4C* and *CYCS*) were upregulated (Fig. 1A). Based on PRGs, we performed a PPI as well as a correlation analysis of expression levels (Fig. 1B, C).

3.2. Classification of tumor

We observed 2 alternative cluster patterns based on PRG expression levels in a TCGA cohort of 178 patients with PC using the unsupervised clustering approach (Fig. 2A). In the typing heatmap (Fig. 2B), most genes were shown to be upregulated in cluster 1 and characteristics cliniques, including tumor grade, age, sex, stage, and tumor, node, metastasis, classification, showed no difference between the 2 clusters. Significant differences in OS time were compared between the 2 clusters, with cluster 2 outperforming cluster 1 in survival time (Fig. 2C).

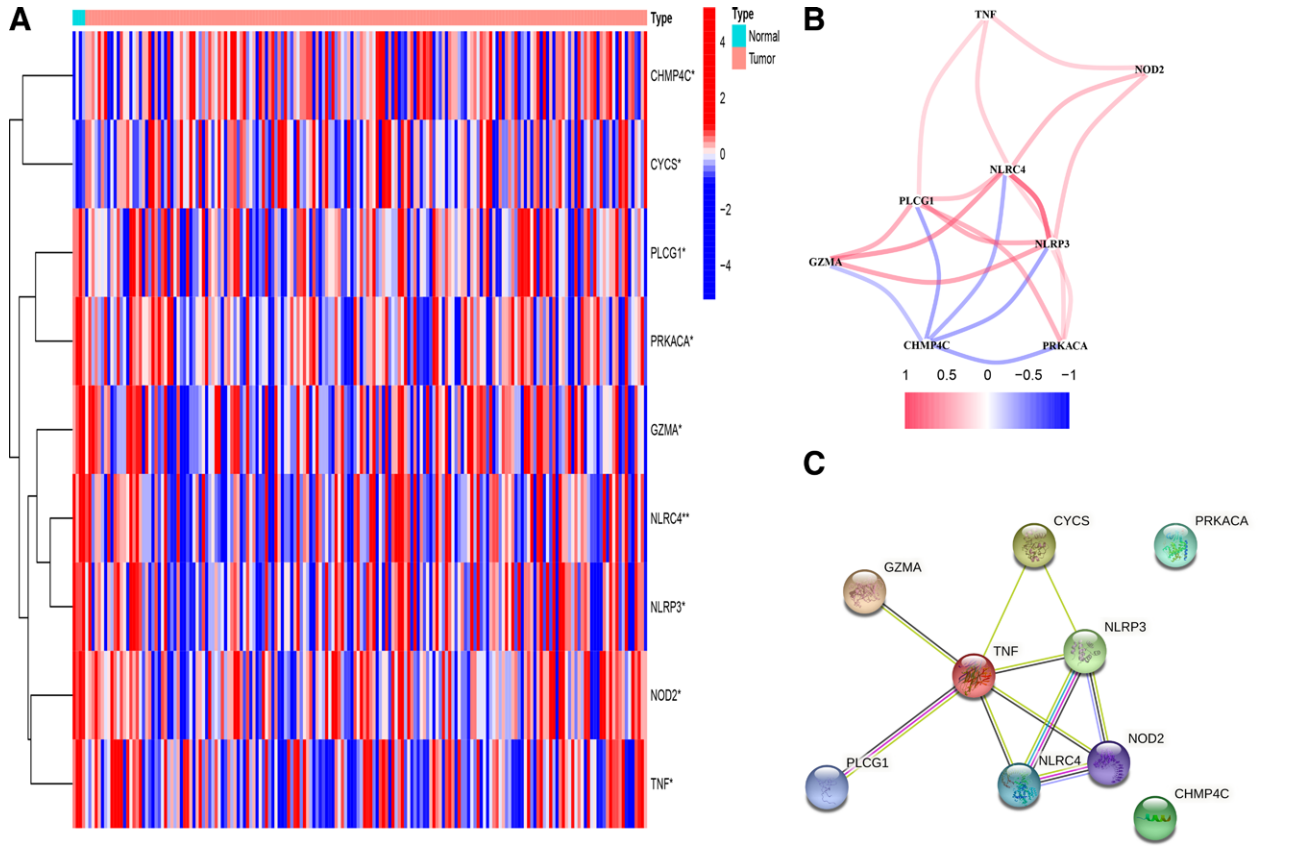

Figure 1. The nine differentially expressed PRGs and the interactions among them. A. Heatmap of the nine PRGs between the normal and the tumor tissues (red: high expression level; blue: low expression level), (*$P < .05$; **$P < .01$). B. The correlation network of the nine PRGs (red line: positive correlation; blue line: negative correlation). C. PPI network of the PRGs (interaction score = 0.9).PPI = protein-protein interaction, PRGs = pyroptosis-related genes.

3.3. Construction of a prognostic model in TCGA

First, we screened 17 PRGs with prognostic value by performing univariate Cox regression analysis. Based on the optimal λ-value, LASSO-Cox regression analysis was performed, and eventually, 5 PRGs (Fig. 3A, B) were screened to develop a prognostic model.

$$\begin{aligned}\text{Risk score} = {} & (0.206 \times \textit{CHMP4C expression}) \\ & + (0.235 \times \textit{BAK1 expression}) \\ & + (0.245 \times \textit{IL18 expression}) \\ & + (0.068 \times \textit{TP63 expression}) \\ & + (0.113 \times \textit{NLRP2 expression})\end{aligned}$$

Patients in the training model were separated into low- and high-risk categories in accordance with their median risk score. The OS curves demonstrated that patients with PC who were classified as high-risk had a lower likelihood of survival than those classified as low-risk ($P < .01$, Fig. 3C). The area under curve predictive values of the training model for 1, 3, and 5 year survival rates were 0.800, 0.805, and 0.721, respectively ($P < .01$, Fig. 3D). The risk graph (Fig. 3E, F) showed that as the risk factor rose (from left to right), the number of patients who died also went up. PCA and t-SNE analysis revealed that these signatures were well-distinguished between patients with different risk scores (Fig. 3G, H).

3.4. Validation of the prognostic model on GEO database

Transcriptome data in the GEO database was normalized and then combined with the survival data. Thirty patients were classed as low-risk, while 33 were classified as high-risk, according to the training group's risk score. Following that, the GEO cohort was utilized to verify the TCGA cohort's prognostic model. The KM survival curve showed that patients in the high-risk group had shorter survival times than those in the low-risk group ($P = .030$, Fig. 4A). Moreover, ROC curves (Fig. 4B) showed that the 1-, 2-, and 3-years of survival times were 0.741, 0.683, and 0.705, respectively. These results were similar to those of the training group, confirming the good predictive efficacy of TCGA cohort model. The results of the risk curve, survival time, PCA, and t-SNE (Fig. 4C, D, E, F) of the test group showed the same results that were obtained in the training group.

3.5. Independent prognostic value of the risk score

The risk score was an independent predictor of OS in the training group, according to univariate Cox regression analysis (HR = 9.095 [5.061–16.341], $P < .001$, Fig. 5A). Even after adjusting for potential confounding factors, the risk score remained a significant predictor of OS in multivariate Cox regression analysis (HR = 8.094 [4.501–14.553], $P < .001$, Fig. 5B). In addition, the genes and clinical traits in TCGA cohort model were used to construct heat maps of the high- and low-risk groups (Fig. 5C). The heat map showed no differences in clinical traits in the high- and low-risk groups.

3.6. Analysis of enrichment function

Using the "limma" R package, we retrieved DEGs from TCGA and GEO different risk groups using the screening criterion. We conducted GO enrichment and KEGG pathway analyses to better understand the biological activities and pathways linked to

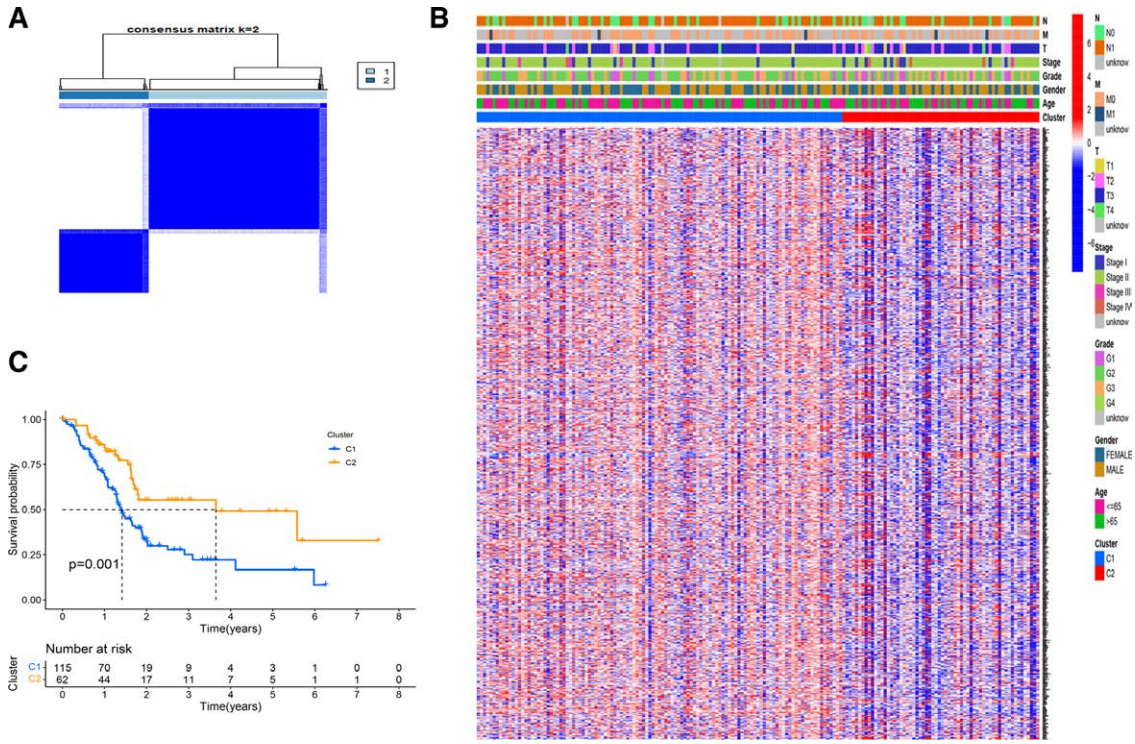

Figure 2. Tumor classification based on the pyroptosis-related DEGs. A. Patients with PC from TCGA cohort were grouped into 2 clusters. B. Heatmap for DEGs and clinicopathological characters between two clusters. C. Kaplan–Meier OS curves for the two clusters.DEGs = extracted differentially expressed genes, OS = overall survival, PC = pancreatic cancer, TCGA = The Cancer Genome Atlas.

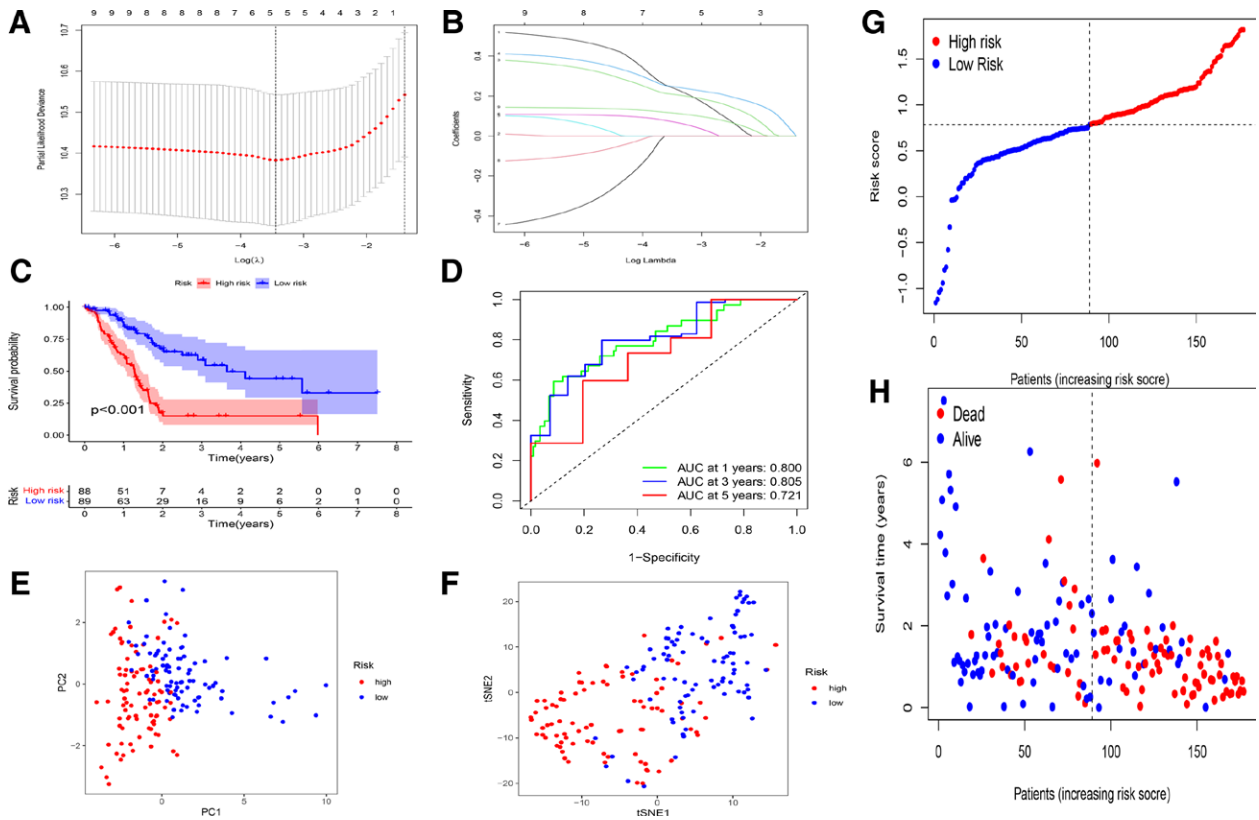

Figure 3. Prognostic model for the TCGA cohort. A. LASSO regression cross-validation. B. LASSO coefficients profiles of 5 genes. C. Kaplan–Meier curves. D. AUC of time-dependent ROC curves. E. PCA plot. F. t-SNE analysis. G. PC patient distribution. H. The survival distribution of PC patients.AUC = area under curve, LASSO = least absolute shrinkage and selection operator, PC = pancreatic cancer, PCA = principal component analysis, ROC = receiver operating characteristic, TCGA = The Cancer Genome Atlas, t-SNE = t-distributed stochastic neighbor embedding.

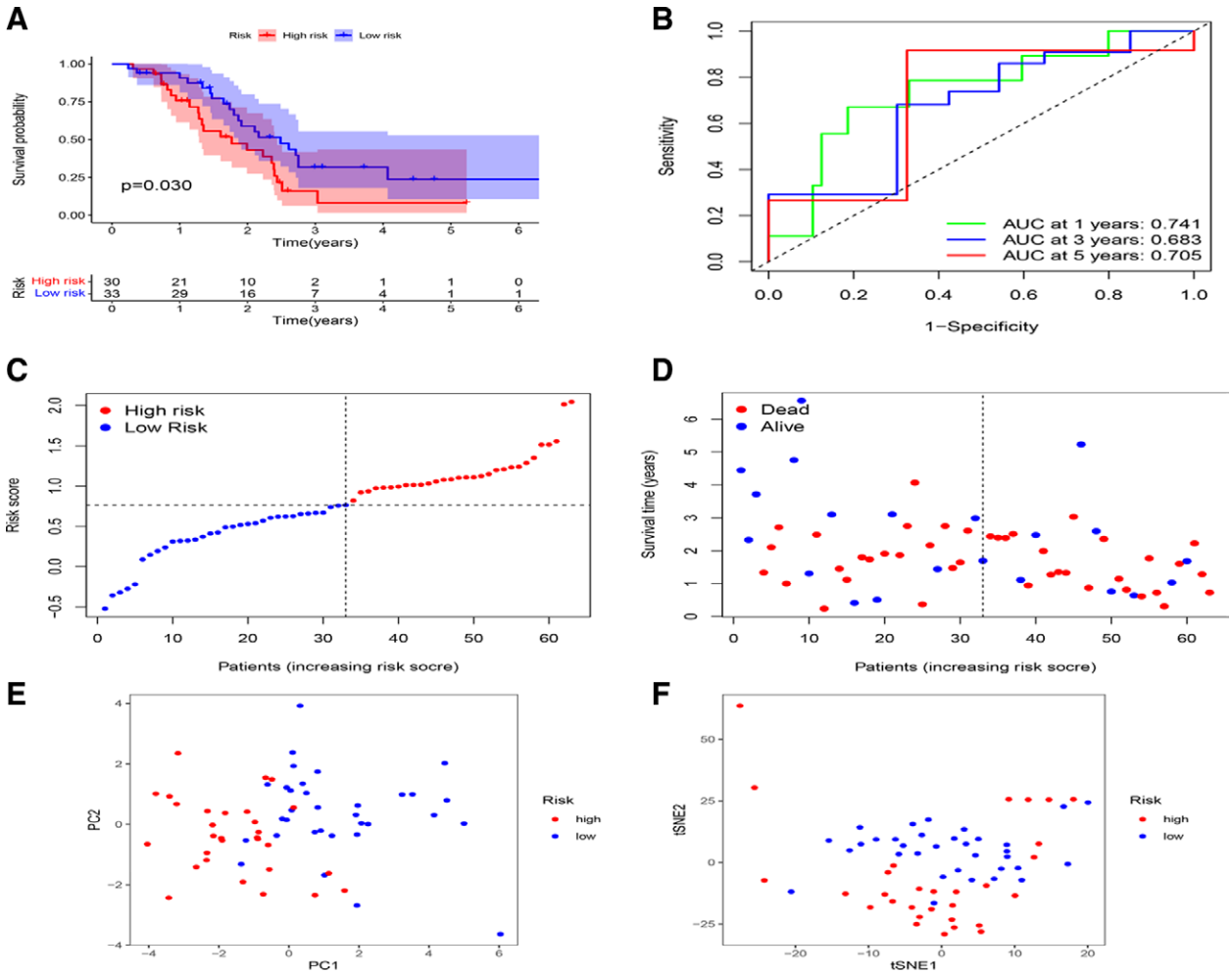

Figure 4. Prognostic model validation in the GEO cohort. A. Kaplan–Meier curves. B. AUC of time-dependent ROC curves. C. PCA plot. D. t-SNE analysis. E. PC patient distribution. F. The survival distribution of PC patients.AUC = area under curve, GEO = Gene Expression Omnibus, PC = pancreatic cancer, PCA = principal component analysis, ROC = receiver operating characteristic, t-SNE = t-distributed stochastic neighbor embedding.

risk score. GO enrichment indicated that the most enriched biological processes, cellular components, and molecular function were organelle fission, cell junction assembly, cell-cell junction, collagen-containing, and channel activity (Fig. 6A, C). KEGG pathway analysis was mainly enriched in signaling pathways such as the PI3K/AKT, Ras, and p53 signaling pathways and the cell cycle (Fig. 6B, D).

3.7. Comparison of the immune state

We used ssGSEA to score immune activity in TCGA and GEO cohorts. Based on the scores, 16 immune cells and 13 immune-related functions were further analyzed for the two low- and high-risk samples, and the results are presented as box plots. The low-risk subgroup of TCGA cohort (Fig. 7A) generally had higher levels of immune cell infiltration, especially in CD8 + T cells, mast cells, neutrophils, T helper cells, and tumor-infiltrating lymphocytes, than the high-risk subgroup. Eight immunological pathways, including antigen presenting cell co_stimulation stimulation, cytolytic activity, T-cell co-inhibition, T-cell co-stimulation, type I and II interferonI response, major histocompatibility complex class I, and parainflammation, exhibited variations in the high- and low-risk groups (Fig. 7B). Finally, our investigation of the immunological state of the GEO group yielded comparable results (Fig. 7C, D).

4. Discussion

In the present study, we began by elucidating the expression and prognostic significance of PRGs in PC. Differences in the expression levels of nine of these PRGs were found. A consensus cluster analysis of these PRGs yielded 2 clusters that did not differentiate in clinical characteristics but showed significant differences in OS time. We used Cox univariate analysis and LASSO-Cox regression to create a prognosis model for 5 PRGs (*BAK1*, *CHMP4C*, *IL18*, *TP63*, and *NLRP2*) to further investigate their prognostic significance. According to risk scores, patients were divided into high- and low-risk groups, and the models were verified using an external dataset. The results demonstrated a significant difference in overall survival time between patients in the high- and low-risk groups; specifically, the low-risk group had a significantly longer survival time than the high-risk group. Furthermore, the risk score has the potential to be employed as an independent prognostic indicator. Between the low- and high-risk groups, DEGs were shown to be connected with apoptosis, the cell cycle, and immune-related pathways, according to the results of enrichment analysis. Finally, we observed that, when compared to the low-risk group, the high-risk group had fewer levels of invading immune cells and lower levels of activation of immune-related pathways.

BAK1, a member of the Bcl-2 family, is induced by the receptor apoptotic protease in the chitin signaling pathway, which

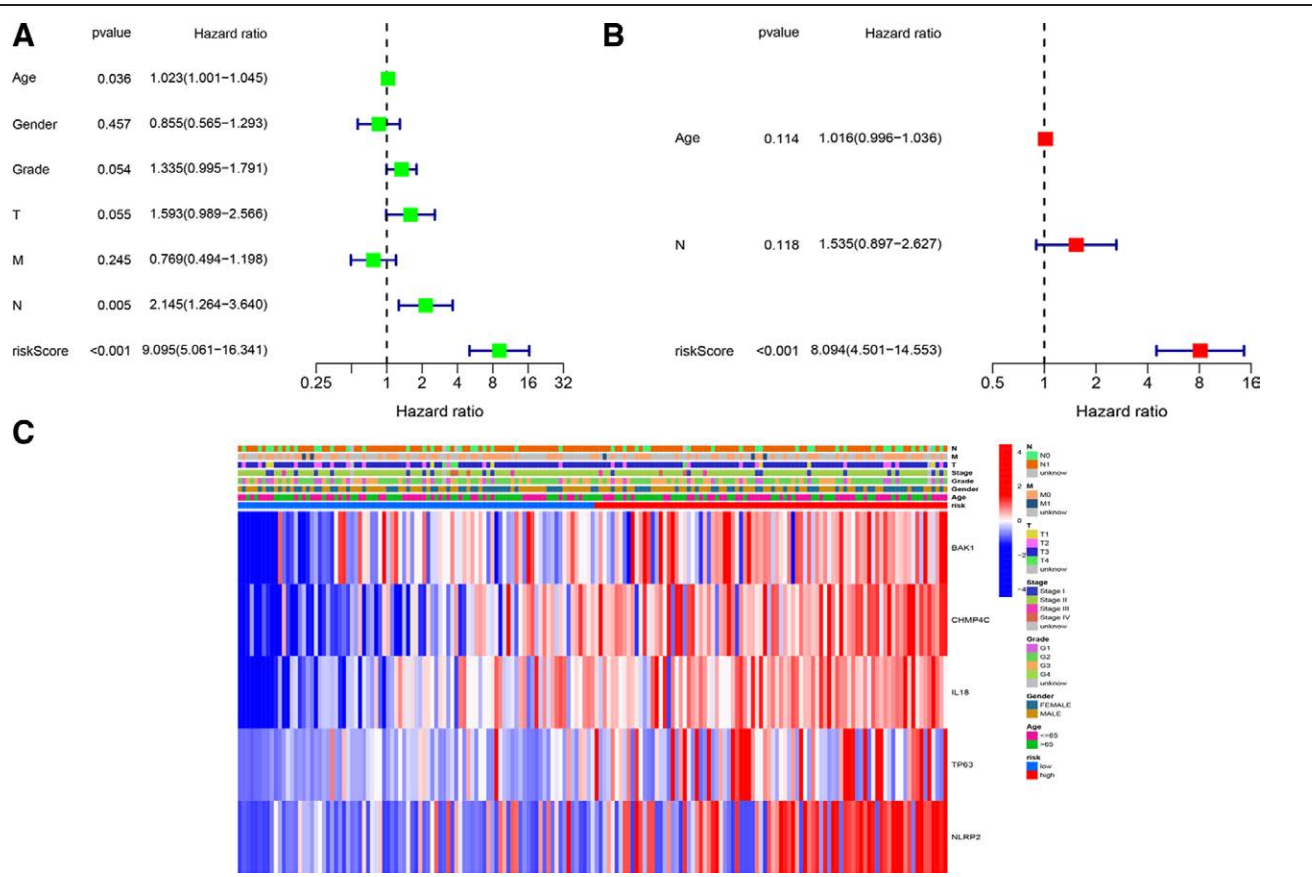

Figure 5. TCGA cohort Cox regression analysis. A. Univariate Analysis. B. Multivariate analysis. C. Heatmap for the clinical-pathological features-risk groups relationship.TCGA = The Cancer Genome Atlas.

inhibits the activity of this receptor kinase and promotes apoptosis.[25] Liu et al found that *BAK1* is activated to form protein pore channels in mitochondria, which releases cytochromes and induces apoptosis.[26] Several studies have reported that *BAK1* is a major cytokine receptor-mediated signal transduction pathway that is widely involved in tumor cell proliferation, differentiation, and apoptosis.[27–29]

Furthermore, *CHMP4C* is also a member of the charged multivesicular body protein family, which is a component of the endosomal sorting complex required for transport III (ESCRT-III).[30,31] ESCRT-III has a function in the cytoplasmic division of daughter cells, and its extracellular vesicles are engaged in a variety of events, including cancer genesis and progression.[32] *CHMP4C* has been shown to play a role in many cancers, such as lung and cervical cancer.[33,34] In our study, *CHMP4C* appears to be an oncogenic gene because it is highly expressed in tumor tissues and high-risk tissues.

Additionally, *IL18* belongs to the IL-1 family and is a widespread pleiotropic cytokine. When synthesized intracellularly, IL18 is a precursor protein of molecular weight. It is then edited by caspase-1 to become a mature, active protein of molecular weight which is secreted extracellularly. IL18 is activated and released from cells and can cause adhesion and aggregation of inflammatory cells and amplify the tissue inflammatory response, which is known to be the main mechanism of pyroptosis.[35] It has been reported that *IL18* has a tumor-promoting effect,[36] but its mechanistic relationship with PC is unclear. In the present study, *IL18* was highly expressed in the high-risk group.

TP63 is an important constituent of the *p53* gene family and has a similar structure and function to *p53*; however, *tp63* has different isoforms, giving it a more complex biological function.[37] In particular, *tp63* is closely associated with processes, such as cell cycle regulation, cell development, and apoptosis, and the roles of different *tp63* isoforms in the proliferation and apoptosis of tumor cells differ. For example, hepatocellular carcinoma Hep3B cells, transduced with the adenovirus-transduced *TAp63α* gene underwent apoptosis in a dose- and time-dependent manner. Moreover, in gastric cancer MKN28 cells, the downregulation of *ΔNp63α* expression inhibited tumor cell proliferation and induced apoptosis.[38] In recent years, it was found that *ΔNp63α* enhances the tolerance of cisplatin-induced apoptosis of PC cells to chemotherapeutic drugs.[39] In this study, *TP63* was highly expressed in the high-risk group, suggesting that this gene may be detrimental to the prognosis of patients with PC.

NLRP2 is a member of the family of intracytoplasmic pattern recognition receptors, NLRPs, which are cytoplasmic proteins. *NLRP2* research in tumors is limited; however, we identified it as a prognosis-related PRG in PC, and it was highly expressed in the high-risk group. Prognosis-related PRGs are able to influence cancer development by regulating processes such as apoptosis, pyroptosis, and inflammatory factor release; however, their specific role in PC is unclear. In the present study, we found that prognosis-related PRGs are closely related to the prognosis of PC and may be important regulators of PC development.

DEGs are primarily implicated in biological processes and signaling pathways associated to apoptosis, cell proliferation, and the cell cycle, such the PI3K/AKT signaling pathway, according to an analysis of DEG enrichment across various risk groups. Cell proliferation, survival, transformation, adhesion, and extracellular matrix breakdown are all regulated by the PI3K/AKT signaling system, which plays a role in cancer and development.[40,41] In terms of immune analysis, lower levels of four immune cells in the high-risk group of TCGA cohort indicated impaired immune function, which was validated in

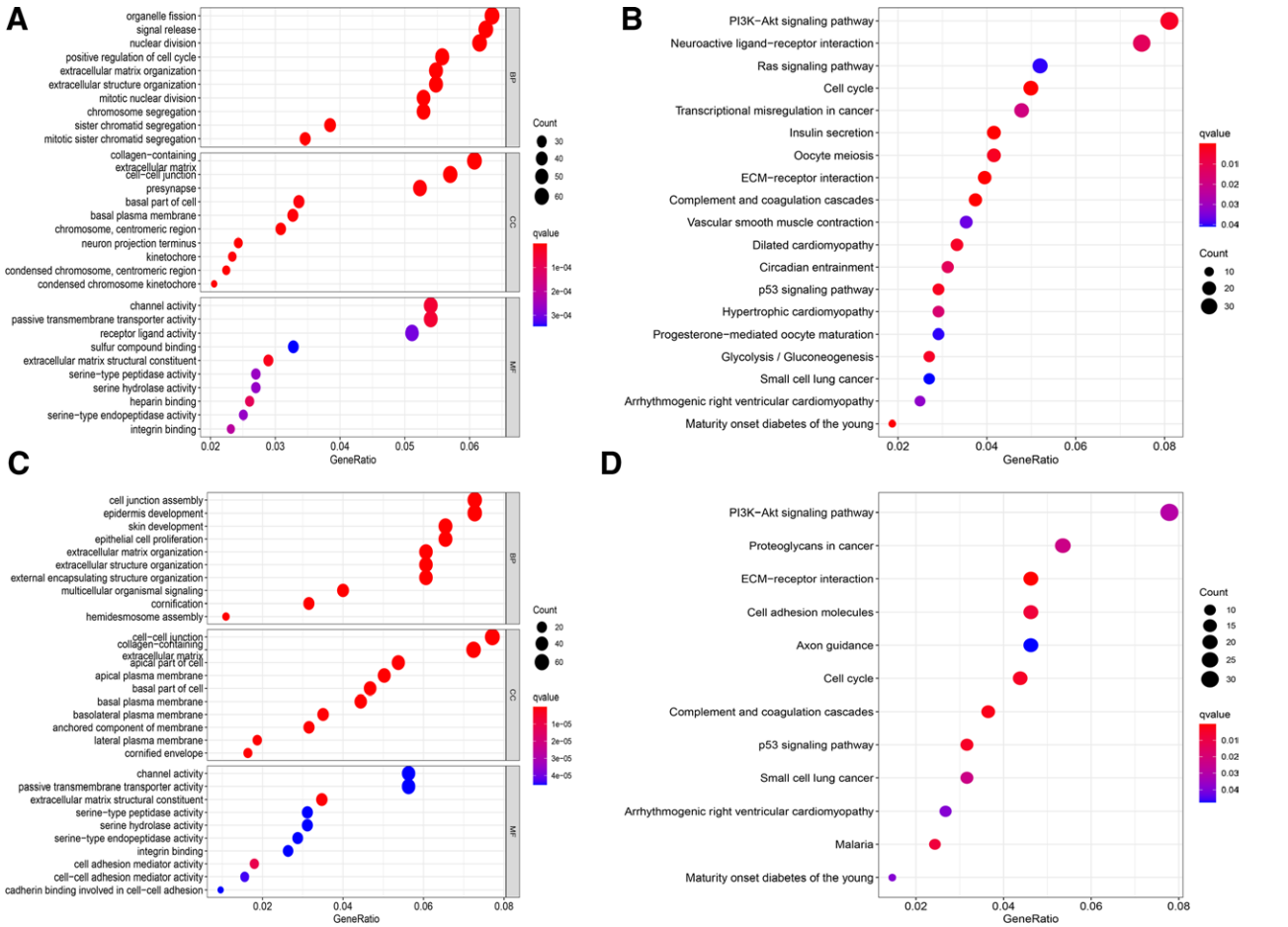

Figure 6. Functional enrichment analysis. (A, B) The TCGA cohort's GO enrichment and KEGG pathways (The color of the bubbles represents the *P* value, while the size denotes the number of genes). (C, D) GO enrichment and KEGG pathways in the GEO cohort.GEO = Gene Expression Omnibus, GO = Gene Ontology, KEGG = Kyoto Encyclopedia of Genes and Genomes, TCGA = The Cancer Genome Atlas.

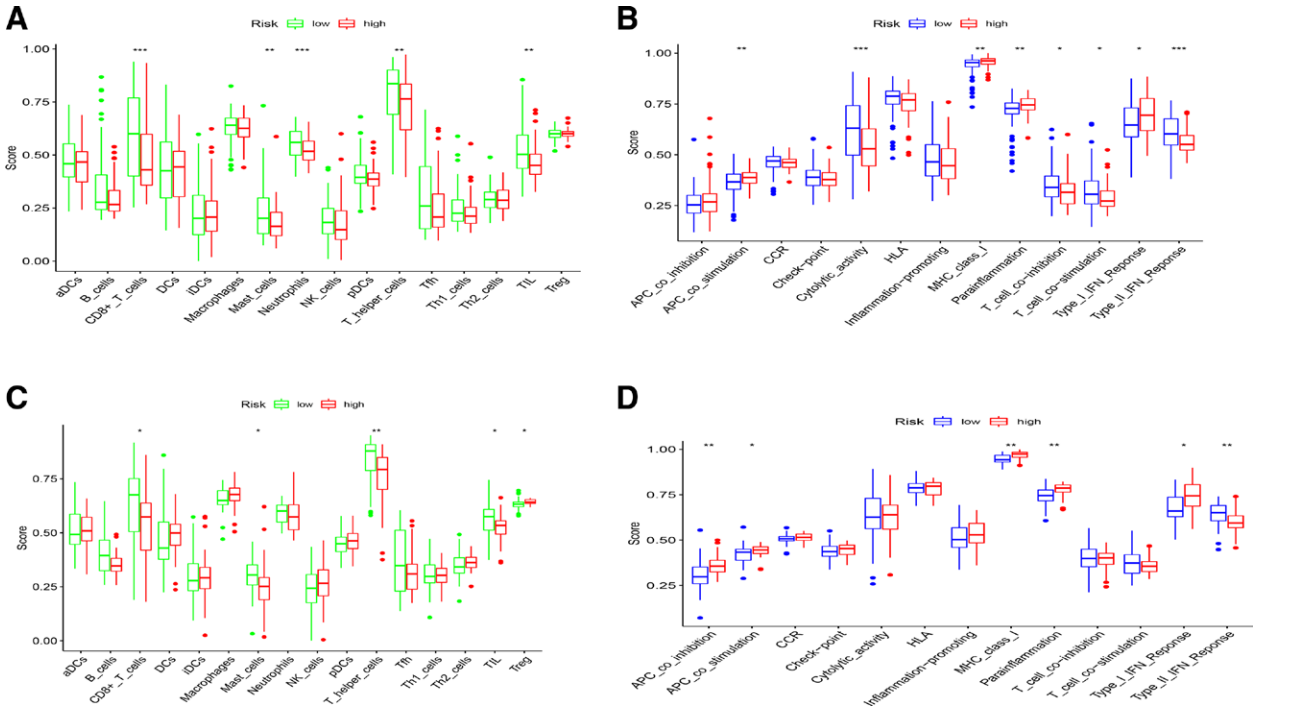

Figure 7. Immunological cells and pathways between low- and high-risk group. (A, B) Comparison of 16 types of immune cells and 13 immune-related pathways in the TCGA cohort. (C, D) Comparison for the GEO cohort. (*$P < .05$; **$P < .01$; ***$P < .001$).GEO = Gene Expression Omnibus, TCGA = The Cancer Genome Atlas.

the GEO cohort. Moreover, immune function status analysis showed that the high-risk group was associated with impaired antitumor immunity. Specifically. the proportion of cytolytic activity, T cell co-inhibition, T cell co-stimulation, and type II interferonI response was lower in the high-risk group of TCGA cohort, suggesting that the anti-tumor immune function was impaired in this group. Based on these findings, poor survival outcomes in high-risk patients may be caused by reduced levels of antitumor immunity.

There have been few research examining the involvement of pyroptosis in the pathophysiology of PC. We were the first to study the prognostic utility of PRGs, laying the groundwork for further research. However, this research has certain limitations: The prognostic model established by PRGs is based on the clinical data and gene expression profile of TCGA, a publicly available database, and must be validated using our own clinical data; The prognostic model incorporates only PRG expression levels, and thus many genes associated with PC prognosis may be excluded.

5. Conclusions

Risk scores generated based on the risk profile of five PRGs were independent risk factors for predicting PC in TCGA and GEO cohorts. The model has good predictive value for PC prognosis and may provide a basis for individualized treatment and prognostic assessment of patients with PC.

Author contributions

Conceptualization: Zhongbo Xu, Guojuan Wang.
Data curation: Wenyan Yu, Guojuan Wang.
Formal analysis: Wenyan Yu.
Methodology: Lin Li.
Software: Wenyan Yu.
Supervision: Lin Li.
Validation: Lin Li.
Writing – original draft: Zhongbo Xu, Guojuan Wang.
Writing – review & editing: Zhongbo Xu.

References

[1] Oettle H, Neuhaus P, Hochhaus A, et al. Adjuvant chemotherapy with gemcitabine and long-term outcomes among patients with resected pancreatic cancer: the CONKO-001 randomized trial. JAMA. 2013;310:1473–81.
[2] Siegel RL, Miller KD, Jemal A. Cancer statistics, 2019. CA Cancer J Clin. 2019;69:7–34.
[3] Lin QJ, Yang F, Jin C, et al. Current status and progress of pancreatic cancer in China. World J Gastroenterol. 2015;21:7988–8003.
[4] Gromisch C, Qadan M, Machado MA, et al. Pancreatic adenocarcinoma: unconventional approaches for an unconventional disease. Cancer Res. 2020;80:3179–92.
[5] Neoptolemos JP, Palmer DH, Ghaneh P, et al. Comparison of adjuvant gemcitabine and capecitabine with gemcitabine monotherapy in patients with resected pancreatic cancer (ESPAC-4): a multicentre, open-label, randomised, phase 3 trial. Lancet. 2017;389:1011–24.
[6] D'Arcy MS. Cell death: a review of the major forms of apoptosis, necrosis and autophagy. Cell Biol Int. 2019;43:582–92.
[7] Shi J, Zhao Y, Wang K, et al. Cleavage of GSDMD by inflammatory caspases determines pyroptotic cell death. Nature. 2015;526:660–5.
[8] Sborgi L, Ruhl S, Mulvihill E, et al. GSDMD membrane pore formation constitutes the mechanism of pyroptotic cell death. EMBO J. 2016;35:1766–78.
[9] Yu P, Zhang X, Liu N, et al. Pyroptosis: mechanisms and diseases. Signal Transduct Target Ther. 2021;6:128.
[10] Yang X, Chen G, Yu KN, et al. Cold atmospheric plasma induces GSDME-dependent pyroptotic signaling pathway via ROS generation in tumor cells. Cell Death Dis. 2020;11:295.
[11] Zhang Y, Yang J, Wen Z, et al. A novel 3',5'-diprenylated chalcone induces concurrent apoptosis and GSDME-dependent pyroptosis through activating PKCdelta/JNK signal in prostate cancer. Aging (Albany NY). 2020;12:9103–24.
[12] Wang WJ, Chen D, Jiang MZ, et al. Downregulation of gasdermin D promotes gastric cancer proliferation by regulating cell cycle-related proteins. J Dig Dis. 2018;19:74–83.
[13] Yu J, Li S, Qi J, et al. Cleavage of GSDME by caspase-3 determines lobaplatin-induced pyroptosis in colon cancer cells. Cell Death Dis. 2019;10:193.
[14] Chen DT, Davis-Yadley AH, Huang PY, et al. Prognostic fifteen-gene signature for early stage pancreatic ductal adenocarcinoma. PLoS One. 2015;10:e0133562.
[15] Ritchie ME, Phipson B, Wu D, et al. limma powers differential expression analyses for RNA-sequencing and microarray studies. Nucleic Acids Res. 2015;43:e47.
[16] Al Mamun A, Mimi AA, Aziz MA, et al. Role of pyroptosis in cancer and its therapeutic regulation. Eur J Pharmacol. 2021;910:174444.
[17] Ju X, Yang Z, Zhang H, Wang Q. Role of pyroptosis in cancer cells and clinical applications. Biochimie. 2021;185:78–86.
[18] Li L, Li Y, Bai Y. Role of GSDMB in pyroptosis and cancer. Cancer Manag Res. 2020;12:3033–43.
[19] Xia X, Wang X, Cheng Z, et al. The role of pyroptosis in cancer: pro-cancer or pro-"host"? Cell Death Dis. 2019;10:650.
[20] Shao W, Yang Z, Fu Y, et al. The pyroptosis-related signature predicts prognosis and indicates immune microenvironment infiltration in gastric cancer. Front Cell Dev Biol. 2021;9:676485.
[21] Szklarczyk D, Gable AL, Nastou KC, et al. The STRING database in 2021: customizable protein-protein networks, and functional characterization of user-uploaded gene/measurement sets. Nucleic Acids Res. 2021;49:D605–12.
[22] Wilkerson MD, Hayes DN. ConsensusClusterPlus: a class discovery tool with confidence assessments and item tracking. Bioinformatics. 2010;26:1572–3.
[23] Engebretsen S, Bohlin J. Statistical predictions with glmnet. Clin Epigenetics. 2019;11:123.
[24] Wu T, Hu E, Xu S, et al. clusterProfiler 4.0: a universal enrichment tool for interpreting omics data. Innovation (N Y). 2021;2:100141.
[25] Liu P, Chang F, Zhang T, et al. Downregulation of microRNA-125a is involved in intervertebral disc degeneration by targeting pro-apoptotic Bcl-2 antagonist killer 1. Iran J Basic Med Sci. 2017;20:1260–7.
[26] Liu J, Liu W, Lu Y, et al. Piperlongumine restores the balance of autophagy and apoptosis by increasing BCL2 phosphorylation in rotenone-induced Parkinson disease models. Autophagy. 2018;14:845–61.
[27] Liu C, Zhang A, Cheng L, et al. miR410 regulates apoptosis by targeting Bak1 in human colorectal cancer cells. Mol Med Rep. 2016;14:467–73.
[28] Gu X, Wang J, Luo Y, et al. Down-regulation of miR-150 induces cell proliferation inhibition and apoptosis in non-small-cell lung cancer by targeting BAK1 in vitro. Tumour Biol. 2014;35:5287–93.
[29] Wang Y, Cai N, Wu X, et al. OCT4 promotes tumorigenesis and inhibits apoptosis of cervical cancer cells by miR-125b/BAK1 pathway. Cell Death Dis. 2013;4:e760.
[30] Petsalaki E, Dandoulaki M, Zachos G. The ESCRT protein Chmp4c regulates mitotic spindle checkpoint signaling. J Cell Biol. 2018;217:861–76.
[31] Petsalaki E, Zachos G. CHMP4C: a novel regulator of the mitotic spindle checkpoint. Mol Cell Oncol. 2018;5:e1445944.
[32] Juan T, Furthauer M. Biogenesis and function of ESCRT-dependent extracellular vesicles. Semin Cell Dev Biol. 2018;74:66–77.
[33] Lin SL, Wang M, Cao QQ, et al. Chromatin modified protein 4C (CHMP4C) facilitates the malignant development of cervical cancer cells. FEBS Open Bio. 2020;10:1295–303.
[34] Liu B, Guo S, Li G, et al. CHMP4C regulates lung squamous carcinogenesis and progression through cell cycle pathway. J Thorac Dis. 2021;13:4762–74.
[35] Xue Y, Enosi Tuipulotu D, Tan WH, et al. Emerging activators and regulators of inflammasomes and pyroptosis. Trends Immunol. 2019;40:1035–52.
[36] Srivastava S, Salim N, Robertson MJ. Interleukin-18: biology and role in the immunotherapy of cancer. Curr Med Chem. 2010;17:3353–7.
[37] Yang A, Kaghad M, Wang Y, et al. p63, a p53 homolog at 3q27-29, encodes multiple products with transactivating, death-inducing, and dominant-negative activities. Mol Cell. 1998;2:305–16.
[38] Wang H, Liu Z, Li J, et al. DeltaNp63alpha mediates proliferation and apoptosis in human gastric cancer cells by the regulation of GATA-6. Neoplasma. 2012;59:416–23.
[39] Danilov AV, Neupane D, Nagaraja AS, et al. DeltaNp63alpha-mediated induction of epidermal growth factor receptor promotes pancreatic cancer cell growth and chemoresistance. PLoS One. 2011;6:e26815.
[40] Faes S, Dormond O. PI3K and AKT: unfaithful partners in cancer. Int J Mol Sci . 2015;16:21138–52.
[41] Mayer I, Arteaga CL. The PI3K/AKT pathway as a target for cancer treatment. Annu Rev Med. 2016;67:11–28.